

Learning Graph ARMA Processes from Time-Vertex Spectra

Eylem Tuğçe Güneyi, Berkay Yıldız, Abdullah Canbolat and Elif Vural

Abstract—The modeling of time-varying graph signals as stationary time-vertex stochastic processes permits the inference of missing signal values by efficiently employing the correlation patterns of the process across different graph nodes and time instants. In this study, we first propose an algorithm for computing graph autoregressive moving average (graph ARMA) processes based on learning the joint time-vertex power spectral density of the process from its incomplete realizations. Our solution relies on first roughly estimating the joint spectrum of the process from partially observed realizations and then refining this estimate by projecting it onto the spectrum manifold of the ARMA process. We then present a theoretical analysis of the sample complexity of learning graph ARMA processes. Experimental results show that the proposed approach achieves improvement in the time-vertex signal estimation performance in comparison with reference approaches in the literature.

Index Terms—Graph processes, time-vertex processes, time-varying graph signals, joint power spectral density, graph ARMA models

I. INTRODUCTION

MANY modern digital platforms involve the acquisition and analysis of data over networks, while network data has a typically time-varying structure. For instance, measurements acquired on a sensor network or user data in a social network often vary over time. Regarding such data as time-varying graph signals, or *time-vertex* signals, the modeling, analysis and inference of time-varying signals on graphs emerges as a problem of wide interest in today’s world.

In this work, we study both the methodological and the theoretical aspects of the problem of learning parametric stochastic graph processes. The modeling of time-vertex signals via stochastic processes has been addressed in several previous works, where the traditional definition of random processes in regular domains has been extended to graph domains so as to permit the modeling of both graph signals (vertex signals) [1]–[3] and time-vertex signals [4] as stationary stochastic processes. Stationary process models are of potential interest for a wide range of data collections where the correlation patterns between different nodes evolve in line with the topology of the graph, such as data resulting from message passing, diffusion, or filtering operations over irregular networks. In this paper, we adopt a stationary and parametric graph process model for time vertex-signals, namely the graph ARMA process model [5], [6], and study the problem of learning the joint time-vertex spectrum of the process in a parametric form from its realizations.

Our contributions in this work are twofold: We first propose an algorithm that learns graph ARMA process models from a collection of time-vertex signals, regarded as independent realizations of the process. We consider a relatively challenging setting where the realizations of the process are assumed to be partially observed, i.e., the time-vertex signals at hand may have missing values at arbitrary time instants and graph nodes. Our method relies on the idea of first obtaining a rough estimate of the time-vertex joint power spectral density (JPSD) of the process from its partially known observations through the estimation of its sample covariance matrix. This rough estimate of the JPSD is then refined by fitting it the parameters of a graph ARMA process model. While the original graph ARMA model learning problem is difficult to solve as it is highly nonlinear and nonconvex, we relax it into a convex optimization problem through a series of approximations, which can then be solved accurately via semidefinite quadratic linear programming. Once the graph process model is learnt in this way, the initially missing observations of the realizations are estimated from the second-order statistics of the process. Our methodological contribution essentially differs from the previous efforts [4]–[6] in that it is the first method to learn graph ARMA process models by explicitly employing the information of the joint time-vertex spectrum. Experimental results on several real data sets show that the proposed method outperforms the reference approaches in comparison.

Then, our second contribution is a theoretical sample complexity analysis of the problem of learning graph ARMA models from a finite set of realizations. In particular, under mild assumptions over the joint spectrum manifold of the process (such as finite manifold curvature and nonzero tangents), we first show that the JPSD estimation error decreases at rate $O(1/\sqrt{L})$ as the number L of realizations increases. Then, we study the implications of this result on the estimation error of the missing observations of the process and show that the convergence rate of $O(1/\sqrt{L})$ holds also for this case.

The rest of the paper is organized as follows: In Section II, we discuss the related literature. In Section III, we give a brief overview of the theory of stochastic graph processes. Then in Section IV, we present the proposed method for learning graph ARMA processes. In Section V, we present our theoretical sample complexity analysis for learning graph ARMA models. In Section VI we evaluate the performance of our method with experiments, and in Section VII we conclude.

II. RELATED WORK

The inference of graph signals is a well-studied problem that admits a wide scope of solutions. Methods based

on traditional semi-supervised learning techniques typically rely on regularization on graph domains [7]–[9], which have been extended to time-vertex signals in various recent works through smoothness priors along the vertex and the time dimensions [10]–[12]. In the recent years, another common approach for reconstructing graph signals has been the band-limitedness assumption [13]–[16], which has been employed in time-vertex signal inference problems as well [17].

Among the graph signal inference methods relying on stochastic models, stationary process models are of particular interest. The concept of stationarity in classical signal processing theory has first been extended to irregular graph domains in the leading studies [2]–[4], [18]. The common idea in these studies is to explicitly account for the graph topology in the definition of stationarity, differently from traditional multivariate process models [19], [20]. Girault et al. have defined wide sense stationary graph processes [18] via isometric graph translations [1], while the definition of stationarity is based on graph localization operators in [2] and graph shift operators in [3]. These works have been extended to time-varying graph signals through the definition of joint time-vertex stationarity in the succeeding studies [4], [21], which show that joint stationarity can be characterized through the time-vertex filtering of white processes [22], [23].

The methods in [2], [4] estimate the joint power spectral density (JPSD) of graph processes through the joint time-vertex Fourier transform of process realizations. While these algorithms use nonparametric representations, in several other works stationary graph processes have been defined via parametric models. The concept of AR (autoregressive) and ARMA (autoregressive moving average) processes traditionally used in the modeling of time-series data has been extended to graph domains in the recent studies [3], [5], [6]. In classical signal processing theory, the computation of ARMA process models for time-series data requires the solution of a nonlinear equation system. Although various techniques exist in the classical literature such as approximations using Durbin’s method or PSD factorization solutions via modified Yule-Walker equations [24], it is not straightforward to adapt these methods to graph domains due to the presence of the vertex dimension in addition to the time dimension. The computation of an ARMA model is a highly nonlinear and nonconvex problem in graph domains, to which approximate solutions have been proposed in the previous studies [3], [6].

Our work essentially differs from these previous approaches in that it aims to learn parametric ARMA graph process models by explicitly matching the process parameters to the joint time-vertex spectrum of the process. We note that, unlike our work, the algorithm in [4] uses a nonparametric process model that does not exploit any other information than joint stationarity; the method in [6] estimates model parameters directly from the observations of the process at different time instants without using the information of the joint time-vertex spectrum; and the scope of [3] is limited to vertex stationarity and does not cover joint time-vertex stationarity.

Compared to the previous studies, our method aims to obtain a more thorough characterization of the process statistics as it explicitly seeks to capture the dependencies between

the time dimension and the vertex dimension of the process through the information of the joint spectrum. Besides this, learning the process characteristics through the estimation of the overall joint spectrum rather than individual realizations of the process gives our method a naturally holistic quality, which provides flexibility in several challenging scenarios where other methods would fail: The proposed method is applicable when the process realizations used for learning the model contain missing observations at arbitrary time instants and vertices (unlike e.g., [4]). Also, our algorithm can employ past observations of the process as well as future ones when inferring the observations at a certain time instant (unlike sequential methods such as [6]). As for the theoretical contributions, the study in [5] presents an analysis of the estimation error of the algorithm therein and reports similar convergence rates to our theoretical results in terms of number of realizations, model order, and process dimensions. However, the setting in [5] is different from ours as it focuses on the joint learning of the graph topology and AR process models by fitting a model directly to the process realizations, while we study the problem of learning ARMA process models based on the estimation of the joint time-vertex spectrum. Lastly, a preliminary version of our study has been presented in [25]. The current paper builds on [25] by significantly extending the experimental results and including a detailed theoretical analysis.

III. BRIEF OVERVIEW OF GRAPH PROCESSES

In this section, we give a brief overview of basic concepts related to the stochastic modeling of time-varying signals on graphs.

A. Graph Signal Processing

We consider an undirected weighted graph model $\mathcal{G} = (\mathcal{V}, \mathcal{E}, W)$ consisting of a set of nodes $\mathcal{V} = \{v_1, v_2, \dots, v_N\}$, a set of undirected edges \mathcal{E} that represents the connections between the nodes (vertices), and a weight matrix $W \in \mathbb{R}^{N \times N}$ representing the edge weights. The degree matrix $D \in \mathbb{R}^{N \times N}$ is defined as a diagonal matrix with entries given by $D_{ii} = \sum_{j=1}^N W_{ij}$. The graph Laplacian matrix is defined as $\mathcal{L}_{\mathcal{G}} = D - W \in \mathbb{R}^{N \times N}$. The graph Laplacian has the eigenvalue decomposition $\mathcal{L}_{\mathcal{G}} = U_{\mathcal{G}} \Lambda_{\mathcal{G}} U_{\mathcal{G}}^T$, where the matrix $U_{\mathcal{G}}$ forms a graph Fourier basis.

A graph signal $x : \mathcal{V} \rightarrow \mathbb{R}$ is a mapping from the set of nodes to real numbers, which can alternatively be represented as an N -dimensional vector $x \in \mathbb{R}^N$ in a graph with N nodes. The graph Fourier transform (GFT) \hat{x} of a graph signal x is obtained by taking its inner product with the Fourier basis vectors [26] as $\hat{x} = U_{\mathcal{G}}^T x$, where $(\cdot)^T$ denotes the transpose of a matrix.

Due to the irregular structures of graphs, the filtering operation on graphs is easier to define in the spectral domain. The relationship between the input x and the output y of a graph filter is given by [26]

$$y = g(\mathcal{L}_{\mathcal{G}})x = U_{\mathcal{G}} g(\Lambda_{\mathcal{G}}) U_{\mathcal{G}}^T x. \quad (1)$$

Here $g : \{0\} \cup \mathbb{R}^+ \rightarrow \mathbb{R}$ is a function representing the filter kernel in the spectral domain, and $g(\Lambda_G)$ is a diagonal matrix with diagonals $g(\lambda_n)$, where λ_n are the eigenvalues of \mathcal{L}_G . The matrix $g(\mathcal{L}_G) \in \mathbb{R}^{N \times N}$ provides the representation of the graph filter in the vertex domain.

B. Graph Wide Sense Stationary Processes

Let $x \in \mathbb{R}^N$ be a random vector representing a graph signal. Then x is called a graph wide sense stationary process if it satisfies the following conditions [2]:

- x has a constant mean, i.e., $E[x] = c \mathbf{1}_N$.
- The covariance matrix of x can be written as a graph filter $\Sigma_x = h(\mathcal{L}_G)$.

Here c is a real constant and the vector $\mathbf{1}_N \in \mathbb{R}^N$ consists of 1's. If a random graph process x is graph wide sense stationary, then due to the second condition above, its covariance matrix Σ_x is jointly diagonalizable with the graph Laplacian as it can be decomposed as $\Sigma_x = U_G h(\Lambda_G) U_G^T$. Here, an important property is that the eigenvalues $h(\lambda_n)$ in the diagonals of $h(\Lambda_G)$ give the power spectral density (PSD) of the process x [2].

C. Joint Time-Vertex Signal Processing

A time-varying graph signal, or a *time-vertex* signal observed on a graph \mathcal{G} during the time instants $t = 1, \dots, T$ can be represented as a matrix $X = [x_1 \ x_2 \ \dots \ x_T] \in \mathbb{R}^{N \times T}$. Here each column $x_t \in \mathbb{R}^N$ of X is a graph signal observed at time t , and each row of X is a time signal observed on a graph node.

The joint time-vertex frequency behavior of time-varying graph signals can be analyzed using the joint Fourier transform [4]. If the matrix X is regarded as a collection of N time signals lying in its rows, the discrete Fourier transform (DFT) of these signals can be obtained as

$$\text{DFT}\{X\} = X \text{conj}(U_T) \quad (2)$$

where U_T is the normalized DFT matrix given by

$$U_T(t, \tau) = \frac{e^{j\omega_\tau t}}{\sqrt{T}}, \quad \omega_\tau = \frac{2\pi(\tau-1)}{T} \text{ for } t, \tau = 1, \dots, T \quad (3)$$

and $\text{conj}(\cdot)$ denotes the complex conjugate of a complex number or matrix. On the other hand, if X is regarded as a collection of T graph signals lying in its columns, the GFT of these signals can be computed as

$$\text{GFT}\{X\} = U_G^T X. \quad (4)$$

The joint Fourier transform (JFT) \hat{X} of a time-vertex signal X is then defined in such a way that it takes the GFT along the node dimension and the DFT along the time dimension [4]

$$\hat{X} = \text{JFT}\{X\} = U_G^T X \text{conj}(U_T). \quad (5)$$

Denoting the vectorized form of a time-vertex signal $X \in \mathbb{R}^{N \times T}$ as $\bar{x} \in \mathbb{R}^{NT}$, the joint Fourier transform can also be expressed as [4]

$$\hat{\bar{x}} = U_J^H \bar{x} \quad (6)$$

where $U_J = U_T \otimes U_G$ is the Kronecker product of U_T and U_G , and $(\cdot)^H$ denotes the Hermitian (transpose conjugate) of a matrix. The filtering of time-vertex signals can similarly be defined in the joint spectral domain through the use of the joint Laplacian operator $\mathcal{L}_J = \mathcal{L}_T \otimes I_N + I_T \otimes \mathcal{L}_G$, where \mathcal{L}_T is the Laplacian of a cyclic graph with eigenvector matrix U_T [4], and $I_N \in \mathbb{R}^{N \times N}$ and $I_T \in \mathbb{R}^{T \times T}$ are identity matrices. Then for a joint graph filter $g(\mathcal{L}_J)$, the relation between the input and output time-vertex signals X and Y can be represented in terms of their vectorized forms as

$$\bar{y} = g(\mathcal{L}_J)\bar{x} = U_J h(\Lambda_G, \Omega) U_J^H \bar{x}. \quad (7)$$

Here $h(\Lambda_G, \Omega)$ is a diagonal matrix with $[h(\Lambda_G, \Omega)]_{ii} = h(\lambda_n, \omega_\tau)$ for $i = (\tau-1)N + n$, hence containing on its diagonals the joint filter kernel values $h(\lambda_n, \omega_\tau)$ representing the desired filter response at graph frequency λ_n and time frequency ω_τ .

D. Joint Time-Vertex Wide Sense Stationary Processes

Let $X \in \mathbb{R}^{N \times T}$ be a random time-vertex process, with vectorized form $\bar{x} \in \mathbb{R}^{NT}$. If X satisfies the following conditions, it is called a joint time-vertex wide sense stationary (JWSS) process [4]:

- \bar{x} has a constant mean $E[\bar{x}] = c \mathbf{1}_{NT}$.
- The covariance matrix $\Sigma_{\bar{x}}$ of the process \bar{x} is a joint time-vertex filter

$$\Sigma_{\bar{x}} = h(\mathcal{L}_G, \mathcal{L}_T) = U_J h(\Lambda_G, \Omega) U_J^H. \quad (8)$$

Hence, if \bar{x} is a JWSS process, the covariance matrix $\Sigma_{\bar{x}}$ of the process has the same eigenvector matrix U_J as the joint Laplacian \mathcal{L}_J . Moreover, the eigenvalues $h(\lambda_n, \omega_\tau)$ of $\Sigma_{\bar{x}}$ give the joint power spectral density (JPSD) of the time-vertex process.

E. Autoregressive Moving Average Graph Processes

The concept of autoregressive moving average (ARMA) filters in classical signal processing has been extended to graph domains in several previous works [6], [23]. A JWSS time-vertex process X can be modeled as an ARMA graph process if it is generated by filtering a zero-mean white process with an ARMA graph filter, where the values $w_t \sim \mathcal{N}(0, I_N)$ of the white process at different time instants t are independent. The graph process x_t at each time t is then related to the past values x_{t-p} of the process and the input white process as [6]

$$x_t = - \sum_{p=1}^P a_p(\mathcal{L}_G) x_{t-p} + \sum_{q=0}^Q b_q(\mathcal{L}_G) w_{t-q} \quad (9)$$

where $a_p(\mathcal{L}_G)$, $b_q(\mathcal{L}_G)$ are graph filters. If $a_p(\mathcal{L}_G)$ and $b_q(\mathcal{L}_G)$ are polynomial filters of the form $a_p(\mathcal{L}_G) = \sum_k a_{pk} \mathcal{L}_G^k$ and $b_q(\mathcal{L}_G) = \sum_m b_{qm} \mathcal{L}_G^m$, where \mathcal{L}_G^k represents the k -th power of the graph Laplacian matrix \mathcal{L}_G , then the ARMA graph process model becomes [6], [23]

$$x_t = - \sum_{p=1}^P \sum_{k=0}^K a_{pk} \mathcal{L}_G^k x_{t-p} + \sum_{q=0}^Q \sum_{m=0}^M b_{qm} \mathcal{L}_G^m w_{t-q}. \quad (10)$$

Here a_{pk} and b_{qm} are the ARMA graph filter coefficients. Taking the JFT of the process X , it can be shown that the time-vertex spectral domain representation of the graph filter in (10) is given by [6], [23]

$$H(\lambda_n, \omega_\tau) = \frac{\sum_{q=0}^Q \sum_{m=0}^M b_{qm} \lambda_n^m e^{-j\omega_\tau q}}{1 + \sum_{p=1}^P \sum_{k=0}^K a_{pk} \lambda_n^k e^{-j\omega_\tau p}}. \quad (11)$$

IV. PROPOSED METHOD FOR LEARNING PARAMETRIC TIME-VERTEX PROCESSES

In this work, we consider a setting where L realizations $\{X^l\}_{l=1}^L$ of a time-vertex process X are available. Each realization $X^l \in \mathbb{R}^{N \times T}$ is assumed to be only partially observed, such that the value X_{it}^l of the realization is known only at some of the graph nodes $i \in \{1, \dots, N\}$ for some of the time instances $t \in \{1, \dots, T\}$. Let I^l denote the index set of node-time pairs for which the realization X^l is observed.

$$I^l = \{(i, t) \mid X_{it}^l \text{ is observed}\}$$

Also, let \bar{I}^l denote the complement of I^l , i.e., the index set for which the observation of the realization X^l is missing. Our aim in this work is to estimate the missing observations $\{X_{it}^l \mid (i, t) \in \bar{I}^l, l = 1, \dots, L\}$, given the available process observations $\{X_{it}^l \mid (i, t) \in I^l, l = 1, \dots, L\}$.

Our approach is based on first obtaining an initial rough estimate $\tilde{\Sigma}_{\bar{x}}$ of the covariance matrix $\Sigma_{\bar{x}}$ (8) from the available process observations, which yields a rough estimate $\tilde{h}(\lambda_n, \omega_\tau)$ of the joint power spectral density. We then learn the ARMA model parameters by fitting the joint time-vertex spectrum (11) of the ARMA filter to the initial estimate $\tilde{h}(\lambda_n, \omega_\tau)$ of the JPSD. An improved estimate of the covariance matrix $\Sigma_{\bar{x}}$ is finally obtained from the learnt ARMA model, from which we infer the initially unknown process values. We discuss these steps in detail in the following sections.

A. Initial Estimation of the JPSD

We first describe the initial estimation of the JPSD, which will be used in the computation of ARMA process models in Section IV-B. We compute the initial JPSD by employing a variant of the algorithm proposed in [4]. The covariance matrix $\Sigma_{\bar{x}}$ of a zero-mean time-vertex process X is given by

$$\Sigma_{\bar{x}} = E[\bar{x}\bar{x}^\top] = \begin{bmatrix} \Sigma_{1,1} & \Sigma_{1,2} & \cdots & \Sigma_{1,T} \\ \Sigma_{2,1} & \Sigma_{2,2} & \cdots & \Sigma_{2,T} \\ \vdots & \vdots & \ddots & \vdots \\ \Sigma_{T,1} & \Sigma_{T,2} & \cdots & \Sigma_{T,T} \end{bmatrix} \quad (12)$$

where $\Sigma_{t,u} = E[x_t x_u^\top]$ stands for the covariance matrix of the values of the process at time instants t and u . When X is a JWSS process, the covariance matrix $\Sigma_{\bar{x}}$ is known to have the following special property, which simplifies its estimation: Each covariance matrix $\Sigma_{t,u}$ is a graph filter $\Sigma_{t,u} = g_{t,u}(\mathcal{L}_G)$, which depends only on the time difference $t - u$. This leads to a block-Toeplitz structure in $\Sigma_{\bar{x}}$ [4]. The observation that any graph filter $g(\mathcal{L}_G)$ needs to be symmetric, as well as the overall covariance matrix $\Sigma_{\bar{x}}$, leads to the equality $\Sigma_{t,u} = \Sigma_{u,t}$. Hence, the estimation of $\Sigma_{\bar{x}}$ boils down to the estimation

of the smaller matrices $\Sigma_\Delta \in \mathbb{R}^{N \times N}$, for $\Delta = 0, 1, \dots, T-1$, where $\Sigma_{t,u} = \Sigma_\Delta$ with $\Delta = |t-u|$. We obtain an estimate $\tilde{\Sigma}_\Delta$ of each Σ_Δ by estimating its entries $[\tilde{\Sigma}_\Delta]_{ij}$ from the sample covariance of the observed process value pairs

$$\{(X_{it}^l, X_{ju}^l) \mid (i, t), (j, u) \in I^l, |t-u| = \Delta, l = 1, \dots, L\}.$$

Once we compute the estimate $\tilde{\Sigma}_{\bar{x}}$ of the covariance matrix $\Sigma_{\bar{x}}$, using the relation in (8), we obtain the initial estimate $\tilde{h}(\lambda_n, \omega_\tau)$ of the JPSD simply by extracting the diagonal entries of the matrix

$$\tilde{h}(\Lambda_G, \Omega) = U_J^H \tilde{\Sigma}_{\bar{x}} U_J. \quad (13)$$

B. Computation of the ARMA Graph Process Model

We now propose our problem formulation for learning an ARMA process model coherent with the initially estimated JPSD. We first rewrite the filter spectrum in (11) as

$$H(\lambda_n, \omega_\tau) = \frac{b^H u_{n,\tau}}{1 + a^H v_{n,\tau}} \quad (14)$$

where the vectors $a \in \mathbb{R}^{P(K+1) \times 1}$ and $b \in \mathbb{R}^{(Q+1)(M+1) \times 1}$ respectively consist of the filter coefficients a_{pk} and b_{qm} as

$$\begin{aligned} a &= [a_{10} \ a_{11} \ \cdots \ a_{pk} \ \cdots \ a_{PK}]^H \\ b &= [b_{00} \ b_{01} \ \cdots \ b_{qm} \ \cdots \ b_{QM}]^H. \end{aligned} \quad (15)$$

The vectors $v_{n,\tau} \in \mathbb{C}^{P(K+1) \times 1}$ and $u_{n,\tau} \in \mathbb{C}^{(Q+1)(M+1) \times 1}$ consist of the constant coefficients

$$\begin{aligned} v_{n,\tau} &= [\lambda_n^0 e^{j\omega_\tau 1} \ \lambda_n^1 e^{j\omega_\tau 1} \ \cdots \ \lambda_n^k e^{j\omega_\tau p} \ \cdots \ \lambda_n^K e^{j\omega_\tau P}]^H \\ u_{n,\tau} &= [\lambda_n^0 e^{j\omega_\tau 0} \ \lambda_n^1 e^{j\omega_\tau 0} \ \cdots \ \lambda_n^m e^{j\omega_\tau q} \ \cdots \ \lambda_n^M e^{j\omega_\tau Q}]^H \end{aligned} \quad (16)$$

where λ_n^k denotes the k -th power of the n -th graph eigenvalue λ_n , and the frequency variables ω_τ are as defined in (3).

Similarly to the filtering of white noise processes in classical signal processing, the JPSD $h(\lambda_n, \omega_\tau)$ of the process is related to the filter spectrum in (11) as [4]

$$h(\lambda_n, \omega_\tau) = |H(\lambda_n, \omega_\tau)|^2 = \left| \frac{b^H u_{n,\tau}}{1 + a^H v_{n,\tau}} \right|^2. \quad (17)$$

We then formulate the estimation of the ARMA model from the initially estimated JPSD $\tilde{h}(\lambda_n, \omega_\tau)$ as

$$\min_{a,b} \sum_{n=1}^N \sum_{\tau=1}^T \left| \left| \frac{b^H u_{n,\tau}}{1 + a^H v_{n,\tau}} \right|^2 - \tilde{h}(\lambda_n, \omega_\tau) \right|^2. \quad (18)$$

Due to the fourth-order dependence of the objective function on the model parameters a and b , the optimization problem in (18) is non-convex with non-unique minima, and hence difficult to solve. In order to develop a convex relaxation of this problem, we first reformulate the relation in (10) as

$$\sum_{p=0}^P \sum_{k=0}^K a_{pk} \mathcal{L}_G^k x_{t-p} = \sum_{q=0}^Q \sum_{m=0}^M b_{qm} \mathcal{L}_G^m w_{t-q} \quad (19)$$

where we set $a_{00} = 1$ and $a_{0k} = 0$ for $k = 1, 2, \dots, K$. This new formulation has the advantage that the joint frequency

response of the resulting graph filter has the relatively simple form

$$H(\lambda_n, \omega_\tau) = \frac{b^H u_{n,\tau}}{a^H v_{n,\tau}} \quad (20)$$

where the vectors $a \in \mathbb{R}^{(P+1)(K+1) \times 1}$ and $v_{n,\tau} \in \mathbb{C}^{(P+1)(K+1) \times 1}$ are redefined as

$$a = [a_{00} \ a_{01} \ \cdots \ a_{pk} \ \cdots \ a_{PK}]^H$$

$$v_{n,\tau} = [\lambda_n^0 e^{j\omega_\tau 0} \ \lambda_n^1 e^{j\omega_\tau 0} \ \cdots \ \lambda_n^k e^{j\omega_\tau p} \ \cdots \ \lambda_n^K e^{j\omega_\tau P}]^H$$

and the vectors b and $u_{n,\tau}$ remain as in (15) and (16). The objective function in (18) then becomes

$$\sum_{n=1}^N \sum_{\tau=1}^T \left| \frac{b^H u_{n,\tau}}{a^H v_{n,\tau}} - \tilde{h}(\lambda_n, \omega_\tau) \right|^2$$

$$= \sum_{n=1}^N \sum_{\tau=1}^T \left| \frac{u_{n,\tau}^H b b^H u_{n,\tau}}{v_{n,\tau}^H a a^H v_{n,\tau}} - \tilde{h}(\lambda_n, \omega_\tau) \right|^2. \quad (21)$$

In an effort to remove the term in the denominator, we propose to substitute the above objective with

$$\sum_{n=1}^N \sum_{\tau=1}^T \left| u_{n,\tau}^H b b^H u_{n,\tau} - v_{n,\tau}^H a a^H v_{n,\tau} \tilde{h}(\lambda_n, \omega_\tau) \right|^2. \quad (22)$$

The dependence of this objective on the vectors a and b is still non-convex. We thus propose to relax it into a convex function of the matrices A and B , by defining $A \triangleq a a^H$ and $B \triangleq b b^H$. However, for these definitions to be valid, the matrices A and B must be rank-1 and positive semidefinite. Hence, we get the optimization problem

$$\min_{A,B} \sum_{n=1}^N \sum_{\tau=1}^T \mu(\lambda_n, \omega_\tau) \left| u_{n,\tau}^H B u_{n,\tau} - v_{n,\tau}^H A v_{n,\tau} \tilde{h}(\lambda_n, \omega_\tau) \right|^2$$

$$\text{subject to} \quad \text{rank}(A) = 1, \text{rank}(B) = 1,$$

$$A \in \mathbf{S}_+^{(P+1)(K+1)}, \quad B \in \mathbf{S}_+^{(Q+1)(M+1)},$$

$$a_{00} = 1, \quad a_{0k} = 0 \text{ for } k = 1, 2, \dots, K \quad (23)$$

where \mathbf{S}_+^R denotes the cone of $R \times R$ positive semidefinite matrices. Here $\mu(\cdot, \cdot)$ stands for an optional weight function for adaptively penalizing the error at particular zones of the joint spectrum, which can be chosen as $\mu(\lambda_n, \omega_\tau) = 1$ under no priors. Lastly, we apply a convex relaxation of the rank constraints as follows. The positive semidefinite matrices A and B can be pushed to be low-rank by minimizing the sums of their singular values, or equivalently, their traces $\text{tr}(A)$ and $\text{tr}(B)$. We hence obtain the final form of our optimization problem as

$$\min_{A,B} \sum_{n=1}^N \sum_{\tau=1}^T \mu(\lambda_n, \omega_\tau) \left| u_{n,\tau}^H B u_{n,\tau} - v_{n,\tau}^H A v_{n,\tau} \tilde{h}(\lambda_n, \omega_\tau) \right|^2$$

$$+ \mu_A \text{tr}(A) + \mu_B \text{tr}(B), \quad \text{subject to} \quad A \in \mathbf{S}_+^{(P+1)(K+1)},$$

$$B \in \mathbf{S}_+^{(Q+1)(M+1)}, \quad a_{00} = 1, \quad a_{0k} = 0 \text{ for } k = 1, 2, \dots, K \quad (24)$$

where μ_A and μ_B are positive weight parameters. The objective function in (24) is quadratic and jointly convex in A and B . We also observe that the constraint set consists of linear

equality constraints and the constraint that A and B be positive semidefinite matrices. Hence, (24) is a convex problem that can be solved using convex optimization techniques [27], [28] relying on semidefinite quadratic linear programming [29], [30]. Once the matrices A and B are computed by solving (24), the ARMA model parameter vectors a and b can be recovered through rank-1 decompositions of respectively A and B .

C. Estimation of Missing Observations of the Process

Having estimated the ARMA model parameters a and b as described in Section IV-B, we now discuss the estimation of the missing observations $\{X_{it}^l \mid (i, t) \in \bar{I}^l\}$ of the process. Following the relation in (17), the learnt model parameters a and b provide an improved estimate of the JPSD, which we may denote as $h^*(\lambda_n, \omega_\tau)$. Rearranging $h^*(\lambda_n, \omega_\tau)$ in matrix form as $h^*(\Lambda_{\mathcal{G}}, \Omega)$, we can obtain an improved estimate $\Sigma_{\bar{x}}^*$ of the covariance matrix $\Sigma_{\bar{x}}$ as

$$\Sigma_{\bar{x}}^* = U_J h^*(\Lambda_{\mathcal{G}}, \Omega) U_J^H \quad (25)$$

which follows from the relation in (8).

Finally, denoting the vectorized form of each realization X^l of the time-vertex process as \bar{x}^l , let us form two new vectors \bar{y}^l and \bar{z}^l , consisting respectively of the known and the missing entries of \bar{x}^l , i.e., the process values in the sets $\{X_{it}^l \mid (i, t) \in I^l\}$ and $\{X_{it}^l \mid (i, t) \in \bar{I}^l\}$. The vector of missing process values \bar{z}^l for $l = 1, \dots, L$ can then be estimated as follows with the classical minimum mean square error (MMSE) estimation approach, which is the same as the linear MMSE estimate since \bar{y}^l and \bar{z}^l are jointly Gaussian [4]

$$(\bar{z}^l)^* = (\Sigma_{\bar{z}\bar{y}}^l)^* ((\Sigma_{\bar{y}\bar{y}}^l)^*)^{-1} \bar{y}^l. \quad (26)$$

Here $(\Sigma_{\bar{z}\bar{y}}^l)^*$ and $(\Sigma_{\bar{y}\bar{y}}^l)^*$ respectively denote the estimates of the cross-covariance matrix of \bar{z}^l and \bar{y}^l , and the covariance matrix of \bar{y}^l . These matrices can be formed by extracting the corresponding entries of $\Sigma_{\bar{x}}^*$ for each realization X^l .

We call the proposed method for learning graph ARMA processes from time-vertex joint spectra as JS-ARMA, and give its summary in Algorithm 1.

Algorithm 1 Proposed JS-ARMA Method

- 1: **Input:** Graph \mathcal{G} , available process observations $\{\bar{y}^l\}_{l=1}^L$
 - 2: Compute \tilde{h} from $\{\bar{y}^l\}$ as explained in Section IV-A
 - 3: Compute A and B by solving the optimization problem (24)
 - 4: Find a and b through rank-1 decompositions of A and B
 - 5: Compute the JPSD $h^*(\lambda_n, \omega_\tau)$ from a and b using (17)
 - 6: Find the covariance matrix $\Sigma_{\bar{x}}^*$ from the JPSD using the relation (25)
 - 7: Find MMSE estimates $\{(\bar{z}^l)^*\}_{l=1}^L$ of observations using (26)
 - 8: **Output:** Estimated process observations $\{(\bar{z}^l)^*\}_{l=1}^L$
-

D. Complexity Analysis of the Algorithm

Here we analyze the computational complexity of the proposed JS-ARMA method. First, we study the computations required for Step-2 of Algorithm 1. Assuming that the graph Laplacian $\mathcal{L}_{\mathcal{G}}$ is known, the time complexities of computing $U_{\mathcal{G}}$ and $\Lambda_{\mathcal{G}}$ is of $O(N^3)$. The joint Fourier transform matrix U_J is found via the Kronecker product of $U_{\mathcal{G}}$ and U_T with a

complexity of $O(N^2T^2)$. Since $\tilde{\Sigma}_{\bar{x}}$ is a block-Toeplitz covariance matrix, it is computed with a complexity of $O(N^2TL)$. Finally, the initial JPSD estimate \tilde{h} is obtained from (13) with a complexity of $O(N^3T^3)$. Next, in Step-3, the optimization problem (24) can be solved with semidefinite quadratic linear programming, via e.g., the HKM algorithm [29], [30]. As the number of variables and the equality constraints in semidefinite quadratic linear programming scale with NT , the analyses in [29], [30] suggest that the solution of (24) results in polynomial complexity $O(\text{poly}(NT))$. In Step-4, the complexities of the rank-1 decompositions of the matrices A and B are of $O((P+1)^3(K+1)^3)$ and $O((Q+1)^3(M+1)^3)$ respectively. Then, in Step-5, $h^*(\lambda_n, \omega_\tau)$ can be found from (17) with a complexity of $O(NT(PK + QM))$. The covariance matrix in Step-6 can be computed using (25) with $O(N^3T^3)$ operations, and lastly, the complexity of finding the MMSE estimates via (26) in step-7 is of $O(N^3T^3)$. Hence, assuming that the model orders P, K, Q, M are smaller than N and T , the overall complexity of our method can be summarized as $O(\text{poly}(NT))$.

V. SAMPLE COMPLEXITY ANALYSIS OF LEARNING GRAPH ARMA MODELS

In this section we theoretically analyze the sample complexity of learning graph ARMA models. We consider a time-vertex process \bar{x} conforming to the ARMA model (10). We denote as a^0 and b^0 the true but unknown parameter vectors generating the process as defined in (15). Let us represent the overall true parameter vector as $\zeta^0 = [(a^0)^H \ (b^0)^H]^H$. We consider a setting where the initial estimate of the process covariance matrix is obtained from the sample covariance of fully observed L independent realizations $\{\bar{x}^l\}_{l=1}^L$ of the process as

$$\tilde{\Sigma}_{\bar{x}} = \frac{1}{L} \sum_{l=1}^L \bar{x}^l (\bar{x}^l)^\top.$$

The initial covariance estimate $\tilde{\Sigma}_{\bar{x}}$ gives the initial JPSD estimate $\tilde{h}(\Lambda_G, \Omega)$ via (13). In order to make the derivations tractable, we base our analysis on the original form (18) of the objective function. Hence, denoting as

$$h_\zeta(\lambda_n, \omega_\tau) = \left| \frac{b^H u_{n,\tau}}{1 + a^H v_{n,\tau}} \right|^2 \quad (27)$$

the JPSD associated with an arbitrary process parameter vector $\zeta \triangleq [a^H \ b^H]^H \in \mathbb{R}^d$ where $d \triangleq P(K+1) + (Q+1)(M+1)$ denotes the model order, we consider the ARMA process parameter vector

$$\zeta^* = \arg \min_{\zeta \in \mathcal{S}} \sum_{n=1}^N \sum_{\tau=1}^T \left| h_\zeta(\lambda_n, \omega_\tau) - \tilde{h}(\lambda_n, \omega_\tau) \right|^2 \quad (28)$$

that best matches the initial JPSD estimate $\tilde{h}(\lambda_n, \omega_\tau)$ as formulated in (18). Here $\mathcal{S} \subset \mathbb{R}^d$ is assumed to be a compact set of feasible parameter vectors that excludes degenerate a and b vectors of zero norm. The JPSD estimate given by the learnt graph ARMA model is thus $h_{\zeta^*}(\lambda_n, \omega_\tau)$. Our purpose in this section is then to characterize how the deviation between the learnt JPSD $h_{\zeta^*}(\lambda_n, \omega_\tau)$ and the true JPSD $h_{\zeta^0}(\lambda_n, \omega_\tau)$

varies with the number of realizations L and the process properties.

Let us simply denote the vectorized form of the JPSD that corresponds to a parameter vector ζ as

$$h_\zeta \triangleq [h_\zeta(\lambda_1, \omega_1) \ h_\zeta(\lambda_2, \omega_1) \ \dots \ h_\zeta(\lambda_N, \omega_T)]^\top \in \mathbb{R}^{NT}.$$

Let us also similarly denote the vectorized form of the initial JPSD estimate $\tilde{h}(\lambda_n, \omega_\tau)$ as $\tilde{h} \in \mathbb{R}^{NT}$. Before presenting our performance bounds, we make the following mild assumptions: Considering the JPSD manifold $\mathcal{H} \triangleq \{h_\zeta : \zeta \in \mathcal{S}\} \subset \mathbb{R}^{NT}$ parameterized by ζ , we first assume that there exists a positive constant $\mathcal{T} > 0$ such that

$$\left\| \frac{dh_{\zeta+tu}}{dt} \Big|_{t=0} \right\| \geq \mathcal{T} \quad (29)$$

for all $\zeta \in \mathcal{S}$ and all $u \in \mathbb{R}^d$ of unit norm $\|u\| = 1$. Here $t \in \mathbb{R}$, and the vector $\frac{dh_{\zeta+tu}}{dt} \in \mathbb{R}^{NT}$ represents a tangent to the manifold \mathcal{H} , which consists of the derivatives of the entries of $h_{\zeta+tu}$. The constant \mathcal{T} thus stands for a lower bound on the tangent norms of the manifold \mathcal{H} , thus imposing \mathcal{H} to have a non-degenerate geometry free of zero tangents. In Appendix A, we show that, if the length of the process is sufficiently large with respect to the number of process parameters so as to satisfy $NT > d = P(K+1) + (Q+1)(M+1)$, then the existence of \mathcal{T} is a very mild, realistic assumption. We next assume that for each (n, τ) pair, there exists a positive constant $\mathcal{K}_{n,\tau}$ such that

$$\left| \frac{d^2}{dt^2} h_{\zeta+tu}(\lambda_n, \omega_\tau) \right| \leq \mathcal{K}_{n,\tau} \quad (30)$$

for any $\zeta \in \mathcal{S}$, any $u \in \mathbb{R}^d$ with $\|u\| = 1$, and any t with $\zeta + tu \in \mathcal{S}$. We can then define a geometric constant

$$\mathcal{K} = \left(\sum_{n=1}^N \sum_{\tau=1}^T \mathcal{K}_{n,\tau}^2 \right)^{1/2} \quad (31)$$

which can be regarded as a global upper bound on the curvature of the manifold \mathcal{H} . In Appendix A, we also show that such a constant \mathcal{K} exists, provided that the JPSD of the process is finite over \mathcal{S} .

We first study in the following lemma the deviation between the true JPSD h_{ζ^0} of the process and its estimate h_{ζ^*} obtained by solving (28).

Lemma 1. *Let $\tilde{e} \triangleq \tilde{h} - h_{\zeta^0}$ denote the error vector representing the deviation of the initial (sample covariance) JPSD estimate \tilde{h} from the true JPSD h_{ζ^0} . Then the JPSD estimation error of an algorithm solving (28) can be bounded as*

$$\|h_{\zeta^*} - h_{\zeta^0}\| \leq \left(\left(\|\tilde{e}\| + \frac{\mathcal{K}}{2} \|\zeta^* - \zeta^0\|^2 \right)^2 - \|\tilde{h} - h_{\zeta^*}\|^2 \right)^{1/2} \\ + \frac{\mathcal{K}}{2\mathcal{T}^2} \left(\left(\|\tilde{e}\| + \frac{\mathcal{K}}{2} \|\zeta^* - \zeta^0\|^2 \right)^2 - \|\tilde{h} - h_{\zeta^*}\|^2 \right). \quad (32)$$

The proof of the lemma is given in Appendix B. Lemma 1 intuitively states the following: The optimization problem (28) seeks for the projection h_{ζ^*} of the initial JPSD estimate

\tilde{h} on the JPSD manifold \mathcal{H} . Assuming that the curvature \mathcal{K} of the manifold is sufficiently small, this projection operation improves the JPSD estimation performance, since the error $\|h_{\zeta^*} - h_{\zeta^0}\|$ remaining after the projection operation reduces the initial error $\|\tilde{e}\| = \|\tilde{h} - h_{\zeta^0}\|$ by an amount proportional to the distance $\|\tilde{h} - h_{\zeta^*}\|$ of \tilde{h} to the manifold \mathcal{H} . Consequently, the graph ARMA model learnt by solving (28) will perform better than the initial JPSD estimate \tilde{h} relying on the sample covariance matrix of the process.

We are now ready to state our first main result on the sample complexity of learning graph ARMA models.

Theorem 1. *Consider a graph ARMA model learnt by solving (28). Then as the number of realizations L increases, with probability at least $1 - \delta$, the estimation errors of the model parameters and the JPSD decrease at the following rates*

$$\begin{aligned} \|\zeta^* - \zeta^0\| &= O\left(\sqrt{\frac{N^2 T^2 d^4}{L\delta}}\right) \\ \|h_{\zeta^*} - h_{\zeta^0}\| &= O\left(\sqrt{\frac{N^2 T^2 d^4}{L\delta}}\right). \end{aligned} \quad (33)$$

The proof of Theorem 1 is given in Appendix C. In the proof, we first examine the convergence rate of the initial error \tilde{e} . We then build on Lemma 1 to derive the rates of convergence of first the model parameter estimation error $\|\zeta^* - \zeta^0\|$, and then the JPSD estimation error $\|h_{\zeta^*} - h_{\zeta^0}\|$. Theorem 1 states that the estimation error of the JPSD of the process converges at rate $O(1/\sqrt{L})$ with L , confirming that the reliability of the estimate improves as the number of realizations L increases. The estimation error scales with N and T as expected, due to the growth in the dimension of h_{ζ} with process dimensions N and T . Meanwhile, the JPSD estimation error also depends on the model order d , as bounded by the quadratic rate $O(d^2)$. Hence, as d increases, the number of realizations L must also increase so as to measure up to the model order, which can be interpreted as a natural consequence of the fact that training models of higher complexity requires more training data in learning theory.

One may wonder about the implications of Theorem 1 for the estimation of the observations of the process. In line with the setting in Section IV-C, let us consider a partially observed test realization $\bar{x}^\theta \in \mathbb{R}^{NT}$ of the time-vertex process \bar{x} ; and denote as \bar{y}^θ and \bar{z}^θ its components respectively with known and missing entries. Let $\Sigma_{\bar{x}}$ and $\Sigma_{\bar{x}}^*$ stand for the true covariance matrix of the process and its estimate given by the JPSD h_{ζ^*} learnt by solving (28). Similarly, let $\Sigma_{\bar{y}}^\theta$, $\Sigma_{\bar{z}\bar{y}}^\theta$ and $(\Sigma_{\bar{y}}^\theta)^*$, $(\Sigma_{\bar{z}\bar{y}}^\theta)^*$ denote the covariance and cross-covariance matrices obtained by extracting the submatrices of $\Sigma_{\bar{x}}$ and $\Sigma_{\bar{x}}^*$ corresponding to the known and the missing parts of a given test realization \bar{x}^θ . In the following main result, we study the rate of convergence of the estimate of \bar{z}^θ based on the MMSE estimation scheme in (26).

Theorem 2. *For a given test realization \bar{x}^θ with observed component \bar{y}^θ , assume that $\Sigma_{\bar{y}}^\theta$, $(\Sigma_{\bar{y}}^\theta)^*$ and their difference are invertible. Let*

$$(\bar{z}^\theta)^* = (\Sigma_{\bar{z}\bar{y}}^\theta)^* ((\Sigma_{\bar{y}}^\theta)^*)^{-1} \bar{y}^\theta$$

denote the MMSE estimate of the missing component \bar{z}^θ obtained through the covariance matrix $\Sigma_{\bar{x}}^*$ estimated by solving (28); and let

$$(\bar{z}^\theta)^0 = \Sigma_{\bar{z}\bar{y}}^\theta (\Sigma_{\bar{y}}^\theta)^{-1} \bar{y}^\theta$$

denote the oracle estimate given by the true covariance matrix $\Sigma_{\bar{x}}$ of the process. Then, as the number of realizations L increases, $(\bar{z}^\theta)^*$ converges to $(\bar{z}^\theta)^0$; such that with probability at least $1 - \delta$, the deviation between them decreases at rate

$$\|(\bar{z}^\theta)^* - (\bar{z}^\theta)^0\| = O\left(\sqrt{\frac{NTd^2}{L\delta}}\right).$$

The proof of Theorem 2 is given in Appendix D, where the result in Theorem 1 is used to bound the deviation between the MMSE estimates $(\bar{z}^\theta)^*$ and $(\bar{z}^\theta)^0$. Theorem 2 states that as the number of realizations increases, the estimate of the missing process observations obtained with the proposed formulation improve progressively, thus converging to the reference ideal estimate $(\bar{z}^\theta)^0$ one would have if the process covariance matrix was perfectly known. In particular, the estimate $(\bar{z}^\theta)^*$ with the learnt model converges to the ideal estimate $(\bar{z}^\theta)^0$ at rate $O(\sqrt{NTd^2/L\delta})$, whose dependence on L is the same as that of the JPSD convergence rate presented in Theorem 1.

VI. EXPERIMENTAL RESULTS

In this section, we evaluate the performance of our method on real and synthetic time-vertex data sets.

A. Performance and Sensitivity Analysis of JS-ARMA

Here we analyze the sensitivity of the proposed JS-ARMA method to factors such as number of realizations, noise, and algorithm parameters through the following experiments.

1) *Model estimation accuracy:* We begin with analyzing the model estimation performance on a synthetically generated graph ARMA process. We experiment on a real graph topology constructed from the Molène weather data set [18], consisting of $N = 33$ meteorological observation stations each of which is represented as a graph node. We form a 5-NN graph with Gaussian edge weights computed as $W_{ij} = \exp(-\|v_i - v_j\|^2/\sigma^2)$, where $\{v_i\}$ denote the locations of the stations and σ is a scale parameter. We synthetically generate realizations of an ARMA graph process with time length $T = 100$ according to the process model (10) on this topology, where the model order parameters are set as $P = 1$, $K = 1$, $Q = 1$, $M = 0$. The parameter vectors defined in (15) are set to have the ground truth values $a = [-0.5 \ 0.5]^H$ and $b = [0.5 \ 0.5]^H$. The JPSD of the process generated with these parameters is shown in Fig. 1(a) and an example realization of the process is shown in Fig. 1(b)-1(d) at three consecutive time instants.

In order to clearly observe the effect of the number of realizations L on the model estimation accuracy, we learn a model from L complete realizations of the process without any missing observations by solving the relaxed optimization problem (24). The realizations of the process are corrupted with additive white Gaussian noise of several noise levels,

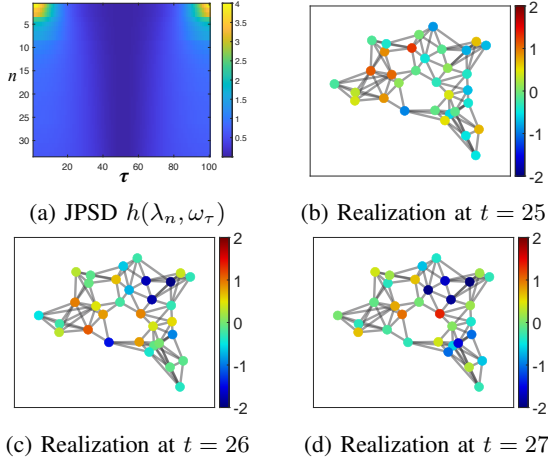


Fig. 1: JPSD and an example realization of the synthetic process

and the variation of the model estimation accuracy with the number of realizations L is studied at each noise level. We evaluate the normalized estimation errors $\|a^* - a^0\|/\|a^0\|$ and $\|b^* - b^0\|/\|b^0\|$ for the model parameter vectors a, b ; and the normalized estimation error $\|h_{\zeta^*} - h_{\zeta^0}\|/\|h_{\zeta^0}\|$ for the JPSD vector, where a^0, b^0, h_{ζ^0} denote the true vectors and a^*, b^*, h_{ζ^*} denote their estimates.

The estimation errors of the parameter vectors a, b and the JPSD are given respectively in Fig. 2(a), 3(a), and 4(a) at different SNR (signal to noise ratio) levels. We observe that even at very high noise levels (i.e., 0dB SNR), the normalized estimation errors of the model parameters remain below 0.15, and that of the JPSD remains below 0.3. An SNR value of 10dB is sufficient to provide a model estimation accuracy very close to the ideal case of infinite SNR and the estimation errors efficiently converge to 0 as the number of realizations increases. This observation confirms that the convex problem (24) derived from the original non-convex problem (18) through several approximations and relaxations is indeed capable of accurately recovering the true process model (except under extreme noise conditions such as the 0dB-SNR scenario). One can also observe that at sufficiently high SNR, the rate of decrease in the estimation errors with the number of realizations L seems coherent with the theoretical convergence rate of $O(1/\sqrt{L})$ presented in Theorem 1.

2) *Effect of model complexity:* We next study how the number of realizations required for accurate model estimation evolves in relation to the model complexity. 6 different ARMA processes are generated with variable model orders P, K, Q, M on the graph topology used in the first experiment. In order to restrict the scope of the experiment to the estimation of the model parameters a, b , and the JPSD, the ground truth model orders are provided to the algorithm. For each combination of P, K, Q, M , the normalized estimation errors of a, b , and the JPSD are plotted respectively in Fig. 2(b), 3(b), and 4(b). We recall from Theorem 1 that the estimation errors are expected to converge at rate $O(\sqrt{N^2 T^2 d^4}/L)$ as the number of realizations L increases. We observe that at all model

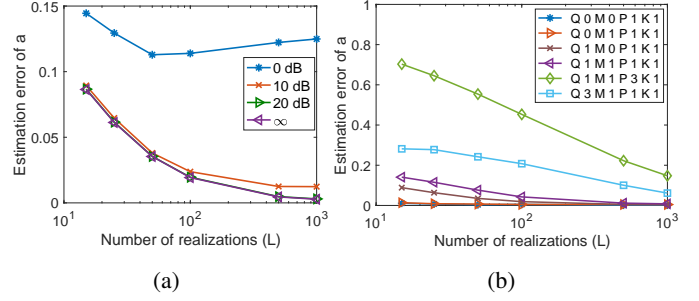


Fig. 2: Variation of the estimation error of a with the number of realizations

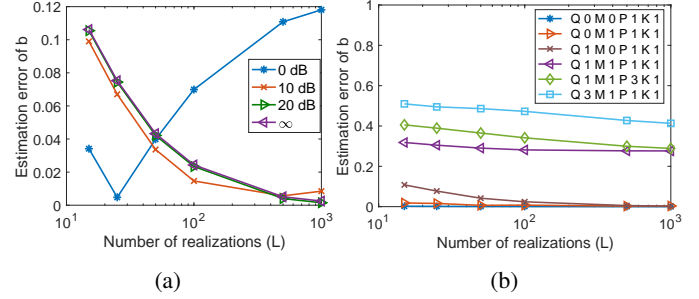


Fig. 3: Variation of the estimation error of b with the number of realizations

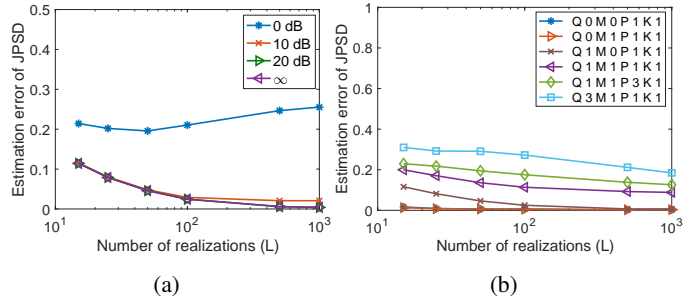


Fig. 4: Variation of the estimation error of the JPSD with the number of realizations

orders the convergence of the estimation errors with L seems coherent with this theoretical result. As for the dependence of the error on the model order, Theorem 1 states that the non-normalized parameter estimation error $\|\zeta^* - \zeta^0\|$ increases with the model dimension $d = P(K+1) + (Q+1)(M+1)$ at a rate bounded by $O(d^2)$. One may then expect the relation $\|\zeta^* - \zeta^0\|/\|\zeta^0\| = O(d^{3/2})$ for the normalized errors. The results in Fig. 2(b)-4(b) indeed confirm that the estimation errors of the model parameters and the JPSD tend to be larger at higher model orders, which is coherent with our theoretical finding. This observation is quite in line with the concept of overfitting in machine learning: A higher model complexity increases the need for training data (i.e. process realizations in our context) in order to properly learn a model.

3) *Sensitivity to weight parameters:* We lastly examine the sensitivity of JS-ARMA to the weight parameters μ_A and

μ_B of the objective function. We conduct the experiment on the COVID-19 pandemic data set described in Section VI-B, which consists of the number of daily new cases reported on the graph of European countries. In each repetition of the experiment, an ARMA process model of order $P = 2$, $K = 0$, $Q = 1$, $M = 1$ is learnt from partially observed process realizations with varying (μ_A, μ_B) combinations, and the missing entries of the realizations are computed via MMSE estimation as explained in Sec. IV-C. The normalized mean errors of the estimates of the missing process observations are computed as

$$NME = \left(\frac{\sum_{l=1}^L \|\bar{z}^l - (\bar{z}^l)^*\|^2}{\sum_{l=1}^L \|\bar{z}^l\|^2} \right)^{1/2} \quad (34)$$

where \bar{z}^l and $(\bar{z}^l)^*$ denote respectively the missing observations and their estimates in (26). The NME values are reported in Table I for different (μ_A, μ_B) combinations, which are averaged over 18 repetitions of the experiment with different random selections of the missing observations and over a range of missing observation ratios varying between 10% and 80%. We first observe that setting μ_A and μ_B to 0 or too small values results in very high estimation errors, which serves as an ablation study, justifying the presence of the $\text{tr}(A)$ and $\text{tr}(B)$ terms in the objective function in (24). Although the minimum NME of 0.17 is attained at relatively high values of μ_A , the intervals $\mu_B \in [10, 100]$, $\mu_A \in [0.001, 0.1]$ define a safe region that provides stable estimation performance. The results on other data sets have led to similar conclusions as well, which are skipped here for brevity.

$\mu_B \backslash \mu_A$	0	0.001	0.01	0.1	1	10	100	1000
0	15.10	11.61	10.01	8.50	5.65	0.22	0.30	23.68
0.001	10.00	9.52	10.68	8.45	7.16	0.22	0.21	20.62
0.01	9.42	9.47	9.61	7.83	5.70	0.22	0.22	21.71
0.1	10.17	10.68	10.75	9.81	4.79	0.22	0.21	11.75
1	8.98	18.84	6.22	3.29	3.12	0.20	0.35	21.29
10	5.39	5.22	4.56	2.67	2.50	0.19	0.26	5.08
100	2.14	2.04	2.00	1.84	1.84	0.33	0.17	0.18
1000	0.43	0.43	0.43	0.42	0.35	0.52	0.17	0.17

TABLE I: Variation of the NME with μ_A and μ_B

B. Comparative Experiments on Real Data Sets

In this section, we evaluate the performance of our method with comparative experiments on the following time-vertex data sets:

1) *Molène weather data set*: The experiment is conducted on hourly weather measurements collected in the Brittany region of France during January 2014 [18]. We experiment on temperature measurements taken on $N = 37$ different weather stations, each of which is represented as a graph node. We construct a 10-NN graph with Gaussian edge weights as explained in Sec. VI-A. We regard each 24-hour measurement sequence as one realization of a time-vertex graph process X with graph size $N = 37$ and time length $T = 24$, obtaining a total of $L = 31$ realizations.

2) *NOAA weather data set*: We experiment on hourly average temperature measurements from the NOAA weather data [31] taken within a year from $N = 246$ weather stations

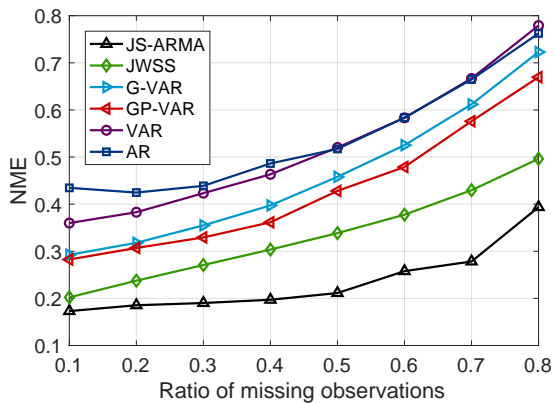
across the United States. Each weather station is considered as a graph node and a 7-NN graph is constructed with Gaussian edge weights. The 24-hour measurement sequences averaged over each week are regarded as a realization of the process. The experiments are therefore conducted on $L = 52$ realizations of a process of time length $T = 24$.

3) *COVID-19 pandemic data set*: The experiments with COVID-19 data [32] are done on the number of daily new cases per country between February 15, 2020 and July 5, 2021. We include the $N = 37$ European countries with highest populations in the experiment, where each country is considered as a graph node. A 4-NN graph is constructed with Gaussian edge weights based on a hybrid distance measure that accounts for both the geographical proximities and the number of flights (accessed through [33]) between each pair of countries. The number of daily new cases are normalized by country populations and smoothed with a moving average filter over a time window of 7 days. The time length of the process is taken as $T = 21$ days (three weeks). The experiments are conducted on $L = 23$ realizations of the process.

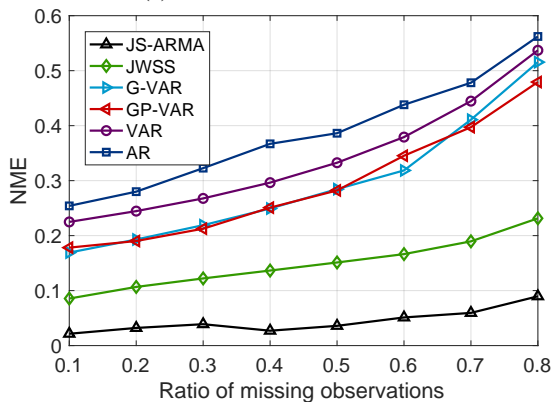
In the experiments, we consider each process realization to have a set of missing observations with randomly selected time and vertex indices. We learn a process model from the known observations by solving (24). The weight function $\mu(\lambda_n, \omega_\tau)$ in (24) is set to be a Gaussian function that penalizes the error at low frequencies more severely, where the spectrum of most real graph processes is likely to be concentrated in practice. The MMSE estimate of the missing observations are then found as discussed in Section IV-C. We compare the estimation performance of the proposed JS-ARMA method with the following approaches: Non-parametric JWSS process models¹ (JWSS) [4], graph vector autoregressive recursions (G-VAR) [6], graph polynomial vector autoregressive recursions (GP-VAR) [6], vector autoregressive process models (VAR) [19], and prediction with an AR time process model (AR) [24]. Half of the known process observations is used for validation for all algorithms that require the tuning of hyperparameters such as model orders and weight parameters.

The performances of the algorithms are compared with respect to the normalized mean error (NME) of the estimates of the missing observations as defined in (34). The variation of the NME with respect to the ratio of missing observations is presented in Fig. 5(a), 5(b), and 5(c) respectively for the Molène, NOAA, and the COVID-19 data sets for all algorithms. We observe that methods based on graph process models perform better than the VAR and AR models most of the time, which treat the data as individual time series and do not make use of the information of the graph topology. Regarding the comparison among the graph-based methods, it is interesting to note that the proposed JS-ARMA method and the JWSS method, which compute models based on the time-vertex joint spectrum of the process, provide better estimation performance than the G-VAR and the GP-VAR methods in general, which do not exploit the information of the joint

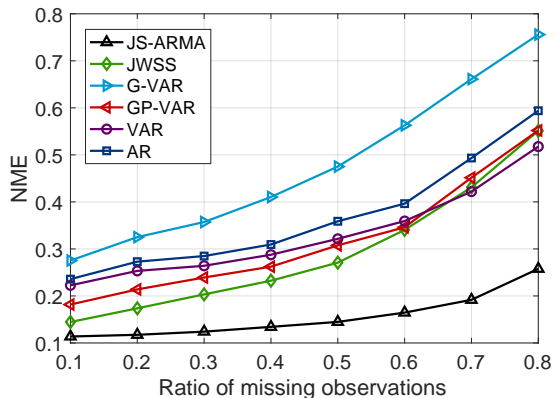
¹As the computation of the JFT is not possible in this setting with missing process observations, we use a variant of the original method [4] by estimating the JPSD from the covariance matrix as in (13) and refining it by extracting its diagonal entries.



(a) Molène weather data set



(b) NOAA weather data set



(c) COVID-19 data set

Fig. 5: Estimation errors of the missing observations for the compared methods

spectrum. This confirms the expectation that the joint time-vertex spectrum of a time-varying graph signal may provide critical information about its characteristics that cannot be captured with only vertex-based frequency analysis. The proposed JS-ARMA method clearly outperforms JWSS and the other methods in comparison. This demonstrates the success of parametric graph process models in achieving higher modeling accuracy in comparison with non-parametric alternatives (e.g. JS-ARMA vs. JWSS) in settings with incomplete process realizations. As parametric methods involve models of smaller complexity compared to non-parametric methods, this may

serve as an advantage in scenarios with limited availability of data. An overall consideration of our experimental results indicates that the proposed JS-ARMA method is able to successfully combine the efficacy of parametric process models with the information of the time-vertex joint spectral characteristics of the data.

VII. CONCLUSION

We have proposed a method for learning parametric stationary graph process models from time-vertex data sets. Our solution is based on fitting the parameters of a graph ARMA model to an initial rough estimate of the joint time-vertex spectrum of the process computed from possibly incomplete realizations of the process. As a second contribution, we have presented a theoretical analysis of the sample complexity of learning graph ARMA processes from realizations of the process. The signal estimation performance of the proposed method has been shown to outperform reference approaches in the literature with experiments on several real time-vertex data sets. The extension of the current study to time-varying graph structures or big network topologies are among the possible future directions of interest.

APPENDIX A: EXISTENCE OF THE CONSTANTS \mathcal{T} AND \mathcal{K}

In this section, we discuss the existence of the geometric constants used in our sample complexity bounds. We first begin with the constant \mathcal{T} . We observe that the derivative of the JPSD $h_{\zeta+tu}(\lambda_n, \omega_\tau)$ at $t = 0$ can be expressed in the form

$$\left. \frac{d}{dt} h_{\zeta+tu}(\lambda_n, \omega_\tau) \right|_{t=0} = (r_\zeta(\lambda_n, \omega_\tau))^\top u \quad (35)$$

where the vector $r_\zeta(\lambda_n, \omega_\tau) \in \mathbb{R}^d$ is defined as

$$\frac{2}{|1 + a^\top v_{n,\tau}|^4} \begin{bmatrix} -|b^\top u_{n,\tau}|^2 (Re\{v_{n,\tau}\} + Re\{v_{n,\tau} v_{n,\tau}^H\} a) \\ |1 + a^\top v_{n,\tau}|^2 Re\{u_{n,\tau} u_{n,\tau}^H\} b \end{bmatrix} \quad (36)$$

for each frequency pair (λ_n, ω_τ) . The tangent vector $\frac{dh_{\zeta+tu}}{dt} \in \mathbb{R}^{NT}$ at $t = 0$ can then be expressed as

$$\left. \frac{dh_{\zeta+tu}}{dt} \right|_{t=0} = R^\top u \quad (37)$$

where the matrix $R \in \mathbb{R}^{d \times NT}$ is defined as

$$R = [r_\zeta(\lambda_1, \omega_1) \ r_\zeta(\lambda_2, \omega_1) \ \dots \ r_\zeta(\lambda_N, \omega_T)]. \quad (38)$$

Now, assuming that the length of the process \bar{x} is large enough to satisfy $NT > d = P(K+1) + (Q+1)(M+1)$, the matrix $R^\top \in \mathbb{R}^{NT \times d}$ is a tall matrix. Hence, the equation system $R^\top u = 0$ is likely to be overdetermined in general and will not have an exact solution for unit-norm vectors with $\|u\| = 1$. This means that norms of the tangent vectors are positive, thus we have $\left\| \frac{dh_{\zeta+tu}}{dt} \right\|_{t=0} > 0$ in general. Hence, provided that $NT > d$, the existence of a positive lower bound \mathcal{T} on the tangent norms is a realistic and mild assumption.

Next, we discuss the existence of the curvature upper bound \mathcal{K} . Let us decompose the unit-norm parameter vector u as $u =$

$[u_a^\top \ u_b^\top]^\top$ such that $u_a \in \mathbb{R}^{P(K+1)}$ and $u_b \in \mathbb{R}^{(Q+1)(M+1)}$. From (27), the JPSD at $\zeta + tu \in \mathcal{S}$ can be written in the form

$$h_{\zeta+tu}(\lambda_n, \omega_\tau) = \frac{\beta(t)}{\alpha(t)} \quad (39)$$

where $\alpha(t) \triangleq |1 + (a + tu_a)^\top v_{n,\tau}|^2$ and $\beta(t) \triangleq |(b + tu_b)^\top u_{n,\tau}|^2$. (The dependence of $\alpha(t)$ and $\beta(t)$ on (λ_n, ω_τ) is omitted from the notation for simplicity.) Since $\zeta + tu$ is assumed to be in the bounded parameter space $\mathcal{S} \in \mathbb{R}^d$, it is easy to show that the first- and second- order derivatives of $\alpha(t)$ and $\beta(t)$ with respect to t are all bounded. Then with a simple inspection of the second derivative expression, we observe that an upper bound on $\left| \frac{d^2}{dt^2} h_{\zeta+tu}(\lambda_n, \omega_\tau) \right|$ exists, provided that the denominator $|\alpha(t)|$ admits a positive lower bound on \mathcal{S} . From our assumption that the spectrum is finite over \mathcal{S} , it follows that $\alpha(t)$ must be nonzero at any $\zeta + tu \in \mathcal{S}$. Since the parameter set \mathcal{S} is assumed to be compact, this implies

$$\inf_{\zeta+tu \in \mathcal{S}} |\alpha(t)| > 0. \quad (40)$$

We thus conclude that for each frequency pair (λ_n, ω_τ) , one can find a finite upper bound $\mathcal{K}_{n,\tau}$ on $\left| \frac{d^2}{dt^2} h_{\zeta+tu}(\lambda_n, \omega_\tau) \right|$, which indicates the existence of a finite global curvature upper bound \mathcal{K} for the JPSD manifold \mathcal{H} .

APPENDIX B: PROOF OF LEMMA 1

Proof. First, we begin with developing a first-order approximation of the JPSD manifold \mathcal{H} . Fixing n and τ , let us regard $h_{\zeta+tu}(\lambda_n, \omega_\tau)$ as a function of $t \in \mathbb{R}$. Taking $\zeta = \zeta^*$, the Taylor expansion of $h_{\zeta^*+tu}(\lambda_n, \omega_\tau)$ around $t = 0$ can be written as

$$\begin{aligned} h_{\zeta^*+tu}(\lambda_n, \omega_\tau) &= h_{\zeta^*}(\lambda_n, \omega_\tau) + t \left(\frac{d}{dr} h_{\zeta^*+ru}(\lambda_n, \omega_\tau) \right) \Big|_{r=0} \\ &\quad + \frac{t^2}{2} \left(\frac{d^2}{dr^2} h_{\zeta^*+ru}(\lambda_n, \omega_\tau) \right) \Big|_{r=r_0} \end{aligned} \quad (41)$$

for some $r_0 \in [0, t]$. Using the bound in (30), we get

$$\begin{aligned} &\left| h_{\zeta^*+tu}(\lambda_n, \omega_\tau) - \left(h_{\zeta^*}(\lambda_n, \omega_\tau) \right. \right. \\ &\quad \left. \left. + t \left(\frac{d}{dr} h_{\zeta^*+ru}(\lambda_n, \omega_\tau) \right) \Big|_{r=0} \right) \right| \leq \frac{t^2}{2} \mathcal{K}_{n,\tau} \end{aligned} \quad (42)$$

for any unit-norm u . Now if we take $t = \|\zeta^0 - \zeta^*\|$ and $u = (\zeta^0 - \zeta^*)/\|\zeta^0 - \zeta^*\|$ in the above equation, we observe that the term h_{ζ^*+tu} becomes equal to the true JPSD h_{ζ^0} , while the term

$$h_{\zeta^*}(\lambda_n, \omega_\tau) + t \left(\frac{d}{dr} h_{\zeta^*+ru}(\lambda_n, \omega_\tau) \right) \Big|_{r=0} \quad (43)$$

can be regarded as a first-order approximation of $h_{\zeta^0} = h_{\zeta^*+tu}$ computed around h_{ζ^*} . Let us denote this first-order approximation of $h_{\zeta^0} \in \mathbb{R}^{NT}$ as $\check{h}_{\zeta^0} \in \mathbb{R}^{NT}$, which is a vector with entries given in (43). Recalling the definition of the curvature upper bound in (31), we then get

$$\|h_{\zeta^0} - \check{h}_{\zeta^0}\| \leq \frac{\mathcal{K}}{2} \|\zeta^0 - \zeta^*\|^2. \quad (44)$$

Next, we observe from (28) that since the manifold point $h_{\zeta^*} \in \mathcal{H}$ is the minimizer of the distance to the initial JPSD estimate \check{h} over the manifold \mathcal{H} , the error vector $\check{h} - h_{\zeta^*}$ must be orthogonal to any tangent to the manifold at $h_{\zeta^*} \in \mathcal{H}$. Since the vector $\check{h}_{\zeta^0} - h_{\zeta^*}$ is tangent to the manifold at point h_{ζ^*} , it is orthogonal to $\check{h} - h_{\zeta^*}$, from which we get

$$\|\check{h} - \check{h}_{\zeta^0}\|^2 = \|\check{h} - h_{\zeta^*}\|^2 + \|h_{\zeta^*} - \check{h}_{\zeta^0}\|^2. \quad (45)$$

Meanwhile, the first term in the above expression can be bounded as

$$\begin{aligned} \|\check{h} - \check{h}_{\zeta^0}\| &= \|\check{h} - h_{\zeta^0} + h_{\zeta^0} - \check{h}_{\zeta^0}\| \leq \|\check{h} - h_{\zeta^0}\| \\ &\quad + \|h_{\zeta^0} - \check{h}_{\zeta^0}\| \leq \|\tilde{e}\| + \frac{\mathcal{K}}{2} \|\zeta^0 - \zeta^*\|^2 \end{aligned} \quad (46)$$

following the bound in (44) and the definition of the initial estimation error \tilde{e} . From (45) and (46), we get

$$\begin{aligned} \|h_{\zeta^*} - \check{h}_{\zeta^0}\|^2 &= \|\check{h} - \check{h}_{\zeta^0}\|^2 - \|\check{h} - h_{\zeta^*}\|^2 \\ &\leq \left(\|\tilde{e}\| + \frac{\mathcal{K}}{2} \|\zeta^0 - \zeta^*\|^2 \right)^2 - \|\check{h} - h_{\zeta^*}\|^2. \end{aligned} \quad (47)$$

We can then obtain

$$\begin{aligned} \|h_{\zeta^*} - h_{\zeta^0}\| &\leq \|h_{\zeta^*} - \check{h}_{\zeta^0}\| + \|\check{h}_{\zeta^0} - h_{\zeta^0}\| \\ &\leq \left(\left(\|\tilde{e}\| + \frac{\mathcal{K}}{2} \|\zeta^0 - \zeta^*\|^2 \right)^2 - \|\check{h} - h_{\zeta^*}\|^2 \right)^{1/2} \\ &\quad + \frac{\mathcal{K}}{2} \|\zeta^0 - \zeta^*\|^2 \end{aligned} \quad (48)$$

where the second equality follows from (47) and (44).

Next, we recall that by taking $t = \|\zeta^0 - \zeta^*\|$ in (43),

$$\check{h}_{\zeta^0} - h_{\zeta^*} = \|\zeta^0 - \zeta^*\| \left(\frac{d}{dr} h_{\zeta^*+ru} \right) \Big|_{r=0} \quad (49)$$

where $\frac{d h_{\zeta^*+ru}}{dr} \Big|_{r=0} \in \mathbb{R}^{NT}$ is the tangent to the manifold \mathcal{H} at point h_{ζ^*} along direction $u = (\zeta^0 - \zeta^*)/\|\zeta^0 - \zeta^*\|$. This gives

$$\begin{aligned} \|\check{h}_{\zeta^0} - h_{\zeta^*}\|^2 &= \|\zeta^0 - \zeta^*\|^2 \left\| \frac{d h_{\zeta^*+ru}}{dr} \Big|_{r=0} \right\|^2 \\ &\leq \left(\|\tilde{e}\| + \frac{\mathcal{K}}{2} \|\zeta^0 - \zeta^*\|^2 \right)^2 - \|\check{h} - h_{\zeta^*}\|^2 \end{aligned} \quad (50)$$

where the inequality follows from (47). Meanwhile, due to the lower bound \mathcal{T} on the tangent norms in (29), we have $\left\| \frac{d h_{\zeta^*+ru}}{dr} \Big|_{r=0} \right\| \geq \mathcal{T}$, which gives from (50)

$$\|\zeta^0 - \zeta^*\|^2 \leq \frac{1}{\mathcal{T}^2} \left(\left(\|\tilde{e}\| + \frac{\mathcal{K}}{2} \|\zeta^0 - \zeta^*\|^2 \right)^2 - \|\check{h} - h_{\zeta^*}\|^2 \right). \quad (51)$$

Using this bound in (48), we get

$$\begin{aligned} \|h_{\zeta^*} - h_{\zeta^0}\| &\leq \left(\left(\|\tilde{e}\| + \frac{\mathcal{K}}{2} \|\zeta^0 - \zeta^*\|^2 \right)^2 - \|\check{h} - h_{\zeta^*}\|^2 \right)^{1/2} \\ &\quad + \frac{\mathcal{K}}{2\mathcal{T}^2} \left(\left(\|\tilde{e}\| + \frac{\mathcal{K}}{2} \|\zeta^0 - \zeta^*\|^2 \right)^2 - \|\check{h} - h_{\zeta^*}\|^2 \right) \end{aligned} \quad (52)$$

which gives the inequality stated in the lemma. \square

APPENDIX C: PROOF OF THEOREM 1

Proof. We begin with studying the rate of decrease of the initial JPSD estimation error $\tilde{e} = \tilde{h} - h_{\zeta^0}$ as the number of realizations L increases. Denoting the true and unknown JPSD of the process as $h_{\zeta^0}(\lambda_n, \omega_\tau)$, and the corresponding matrix form of the JPSD as $h_{\zeta^0}(\Lambda_{\mathcal{G}}, \Omega)$, we have

$$\begin{aligned} E[\|\tilde{e}\|^2] &= E[\|\tilde{h} - h_{\zeta^0}\|^2] \leq E[\|\tilde{h}(\Lambda_{\mathcal{G}}, \Omega) - h_{\zeta^0}(\Lambda_{\mathcal{G}}, \Omega)\|_F^2] \\ &= E[\|U_J^H \tilde{\Sigma}_{\bar{x}} U_J - U_J^H \Sigma_{\bar{x}} U_J\|_F^2] = E[\|\tilde{\Sigma}_{\bar{x}} - \Sigma_{\bar{x}}\|_F^2] \\ &= E[\|L^{-1}\Phi - L^{-1}E[\Phi]\|_F^2] = \frac{1}{L^2} E[\|\Phi - E[\Phi]\|_F^2] \\ &= \frac{1}{L^2} \sum_{i=1}^{NT} \sum_{j=1}^{NT} \text{Var}(\Phi_{ij}) \end{aligned} \quad (53)$$

where we define $\Phi = \sum_{l=1}^L \bar{x}^l (\bar{x}^l)^\top$ and $(\cdot)_{ij}$ denotes the (i, j) -th entry of a matrix. The notation $\|\cdot\|_F$ stands for the Frobenius norm, $\text{Var}(\cdot)$ denotes the variance, and we simply refer to the true covariance matrix of the process as $\Sigma_{\bar{x}}$. Since \bar{x} is assumed to be a Gaussian process in our study, the matrix Φ defined as above has a Wishart distribution with L degrees of freedom, its expectation being given by $E[\Phi] = L\Sigma_{\bar{x}}$. From (53) and the variance of the Wishart distribution, we obtain

$$\begin{aligned} E[\|\tilde{e}\|^2] &\leq \frac{1}{L^2} \sum_{i=1}^{NT} \sum_{j=1}^{NT} L ((\Sigma_{\bar{x}})_{ij}^2 + (\Sigma_{\bar{x}})_{ii}(\Sigma_{\bar{x}})_{jj}) \\ &= \frac{1}{L} (\|\Sigma_{\bar{x}}\|_F^2 + \text{tr}(\Sigma_{\bar{x}})^2) = \frac{1}{L} C_{\zeta^0} \end{aligned} \quad (54)$$

where $C_{\zeta^0} \triangleq \|\Sigma_{\bar{x}}\|_F^2 + \text{tr}(\Sigma_{\bar{x}})^2$ is a constant depending on the model parameters ζ^0 . From Markov's equality for any $\epsilon > 0$ we have

$$P(\|\tilde{e}\|^2 \geq \epsilon^2) \leq \frac{E[\|\tilde{e}\|^2]}{\epsilon^2} \leq \frac{C_{\zeta^0}}{L\epsilon^2}. \quad (55)$$

Here the constant C_{ζ^0} grows at rate $O(N^2T^2)$ with the dimension NT of the process. As for its dependence on the dimension d of the parameter space, we observe from (27) that $h_{\zeta^0}(\lambda_n, \omega_\tau)$ grows at a rate bounded by $O(d^2)$, which implies $\|\Sigma_{\bar{x}}\|_F^2 = \|U_J h_{\zeta^0}(\Lambda_{\mathcal{G}}, \Omega) U_J^H\|_F^2 = \|h_{\zeta^0}(\Lambda_{\mathcal{G}}, \Omega)\|_F^2 = O(d^4)$. Hence, we conclude that $C_{\zeta^0} = O(N^2T^2d^4)$. Defining $\delta = \frac{C_{\zeta^0}}{L\epsilon^2}$ in (55), we get that with probability at least $1 - \delta$,

$$\|\tilde{e}\| \leq \epsilon = \sqrt{\frac{C_{\zeta^0}}{L\delta}} = O\left(\sqrt{\frac{N^2T^2d^4}{L\delta}}\right). \quad (56)$$

Hence, we have shown that the initial JPSD estimation error $\|\tilde{e}\|$ decreases at rate $O(\sqrt{N^2T^2d^4/(L\delta)})$ as L increases. In the sequel, we employ this result to study the rate of convergence of the JPSD estimation error $\|h_{\zeta^*} - h_{\zeta^0}\|$ in (32). We first observe that as h_{ζ^*} is the projection of \tilde{h} onto \mathcal{H} , we have $\|\tilde{h} - h_{\zeta^*}\| \leq \|\tilde{h} - h_{\zeta^0}\| = \|\tilde{e}\|$, which implies from (56)

$$\|\tilde{h} - h_{\zeta^*}\| = O\left(\sqrt{\frac{N^2T^2d^4}{L\delta}}\right). \quad (57)$$

Then, it remains to determine the rate of convergence of the estimation error $\|\zeta^* - \zeta^0\|$ of the process model parameters. We recall from the proof of Lemma 1 that taking $t = \|\zeta^0 - \zeta^*\|$ and $u = (\zeta^0 - \zeta^*)/\|\zeta^0 - \zeta^*\|$ in (41), we have

$$\begin{aligned} h_{\zeta^0} &= h_{\zeta^*} + \|\zeta^0 - \zeta^*\| \left(\frac{d}{dr} h_{\zeta^*+ru} \right) \Big|_{r=0} \\ &\quad + \frac{1}{2} \|\zeta^0 - \zeta^*\|^2 \left(\frac{d^2}{dr^2} h_{\zeta^*+ru} \right) \Big|_{r=r_0} \end{aligned} \quad (58)$$

where the tangent vector $\frac{d h_{\zeta^*+ru}}{dr} \Big|_{r=0} \in \mathbb{R}^{NT}$ and the curvature vector $\frac{d^2 h_{\zeta^*+ru}}{dr^2} \Big|_{r=r_0} \in \mathbb{R}^{NT}$ consist of the first- and the second-order derivatives to the manifold \mathcal{H} . From (58) we get

$$\begin{aligned} \|\zeta^0 - \zeta^*\| &\left\| \frac{d}{dr} h_{\zeta^*+ru} \Big|_{r=0} \right\| \\ &= \left\| h_{\zeta^0} - h_{\zeta^*} - \frac{1}{2} \|\zeta^0 - \zeta^*\|^2 \left(\frac{d^2}{dr^2} h_{\zeta^*+ru} \right) \Big|_{r=r_0} \right\| \\ &\leq \|h_{\zeta^*} - h_{\zeta^0}\| + \frac{1}{2} \|\zeta^0 - \zeta^*\|^2 \left\| \frac{d^2}{dr^2} h_{\zeta^*+ru} \Big|_{r=r_0} \right\|. \end{aligned} \quad (59)$$

Using the bounds (29) and (31) on the norms of the tangent and curvature vectors, we then obtain

$$\|\zeta^0 - \zeta^*\| \leq \frac{1}{\mathcal{T}} \|h_{\zeta^*} - h_{\zeta^0}\| + \frac{\mathcal{K}}{2\mathcal{T}} \|\zeta^0 - \zeta^*\|^2. \quad (60)$$

Now defining in (32)

$$\begin{aligned} \tilde{g} &\triangleq \left(\|\tilde{e}\| + \frac{\mathcal{K}}{2} \|\zeta^0 - \zeta^*\|^2 \right)^2 - \|\tilde{h} - h_{\zeta^*}\|^2 \\ &= \|\tilde{e}\|^2 + \mathcal{K} \|\tilde{e}\| \|\zeta^0 - \zeta^*\|^2 + \frac{\mathcal{K}^2}{4} \|\zeta^0 - \zeta^*\|^4 - \|\tilde{h} - h_{\zeta^*}\|^2 \end{aligned} \quad (61)$$

and recalling the convergence rates (56) and (57), we get

$$\begin{aligned} \tilde{g} &\leq O\left(\frac{N^2T^2d^4}{L\delta}\right) + \mathcal{K} \|\zeta^0 - \zeta^*\|^2 O\left(\sqrt{\frac{N^2T^2d^4}{L\delta}}\right) \\ &\quad + \frac{\mathcal{K}^2}{4} \|\zeta^0 - \zeta^*\|^4. \end{aligned} \quad (62)$$

From Lemma 1, we recall that

$$\|h_{\zeta^*} - h_{\zeta^0}\| \leq \sqrt{\tilde{g}} + \frac{\mathcal{K}}{2\mathcal{T}^2} \tilde{g} \quad (63)$$

which gives from (60)

$$\|\zeta^0 - \zeta^*\| \leq \frac{1}{\mathcal{T}} \left(\sqrt{\tilde{g}} + \frac{\mathcal{K}}{2\mathcal{T}^2} \tilde{g} \right) + \frac{\mathcal{K}}{2\mathcal{T}} \|\zeta^0 - \zeta^*\|^2. \quad (64)$$

In order to determine the rate of convergence of $\|\zeta^0 - \zeta^*\|$, we make the following observations: First, as the number of realizations L increases, we can ignore the effect of the term $\tilde{g}\mathcal{K}/(2\mathcal{T}^2)$ in (64), since the term $\sqrt{\tilde{g}}$ will converge at a slower rate than \tilde{g} . Combining this observation with the bound in (62), we can rewrite (64) as

$$\begin{aligned} \|\zeta^0 - \zeta^*\| &\leq c_1 \left(O\left(\frac{N^2T^2d^4}{L\delta}\right) + \|\zeta^0 - \zeta^*\|^2 O\left(\sqrt{\frac{N^2T^2d^4}{L\delta}}\right) \right) \\ &\quad + c_2 \|\zeta^0 - \zeta^*\|^4 \Big)^{1/2} + c_3 \|\zeta^0 - \zeta^*\|^2 \end{aligned} \quad (65)$$

for some constants c_i 's. We thus observe that $\|\zeta^0 - \zeta^*\|$ can not converge at a rate slower than $O(\sqrt{N^2 T^2 d^4 / (L\delta)})$; otherwise the inequality would be violated for large L . We thus get

$$\|\zeta^0 - \zeta^*\| = O\left(\sqrt{\frac{N^2 T^2 d^4}{L\delta}}\right). \quad (66)$$

Using the convergence rates (56), (57), and (66) in (62), one can find the rate of convergence of the term \tilde{g} . We observe that the curvature parameter \mathcal{K} increases at rate $O(\sqrt{NT})$ as the dimensions N and T grow. Assuming that the number of realizations L is sufficiently large to satisfy the rate $L = \Omega((NT)^{5/2} d^4)$ at large dimensions, one gets $\tilde{g} = O(N^2 T^2 d^4 / (L\delta))$, which finally gives from (32)

$$\|h_{\zeta^*} - h_{\zeta^0}\| = O\left(\sqrt{\frac{N^2 T^2 d^4}{L\delta}}\right).$$

□

APPENDIX D: PROOF OF THEOREM 2

Proof. From the relation (25) between the covariance matrix and the JPSD estimates, we first observe that

$$\begin{aligned} \|\Sigma_{\tilde{x}}^* - \Sigma_{\tilde{x}}\|_F^2 &= \|U_J h_{\zeta^*}(\Lambda_G, \Omega) U_J^H - U_J h_{\zeta^0}(\Lambda_G, \Omega) U_J^H\|_F^2 \\ &= \|h_{\zeta^*}(\Lambda_G, \Omega) - h_{\zeta^0}(\Lambda_G, \Omega)\|_F^2 = \|h_{\zeta^*} - h_{\zeta^0}\|^2 \\ &= O\left(\frac{N^2 T^2 d^4}{L\delta}\right) \end{aligned} \quad (67)$$

with probability at least $1 - \delta$, where the last inequality follows from Theorem 1.

The deviation between the estimates $(\tilde{z}^\theta)^*$ and $(\tilde{z}^\theta)^0$ can be bounded as

$$\begin{aligned} \|(\tilde{z}^\theta)^* - (\tilde{z}^\theta)^0\| &= \|(\Sigma_{\tilde{z}\tilde{y}}^\theta)^* ((\Sigma_{\tilde{y}}^\theta)^*)^{-1} \tilde{y}^\theta - \Sigma_{\tilde{z}\tilde{y}}^\theta (\Sigma_{\tilde{y}}^\theta)^{-1} \tilde{y}^\theta\| \\ &\leq \|(\Sigma_{\tilde{z}\tilde{y}}^\theta)^* ((\Sigma_{\tilde{y}}^\theta)^*)^{-1} - \Sigma_{\tilde{z}\tilde{y}}^\theta (\Sigma_{\tilde{y}}^\theta)^{-1}\| \|\tilde{y}^\theta\| \\ &= \|(\Sigma_{\tilde{z}\tilde{y}}^\theta)^* ((\Sigma_{\tilde{y}}^\theta)^*)^{-1} - \Delta_{\tilde{z}\tilde{y}}^\theta ((\Sigma_{\tilde{y}}^\theta)^*)^{-1} + \Delta_{\tilde{z}\tilde{y}}^\theta ((\Sigma_{\tilde{y}}^\theta)^*)^{-1} \\ &\quad - \Sigma_{\tilde{z}\tilde{y}}^\theta (\Sigma_{\tilde{y}}^\theta)^{-1}\| \|\tilde{y}^\theta\| \\ &\leq \|\Sigma_{\tilde{z}\tilde{y}}^\theta ((\Sigma_{\tilde{y}}^\theta)^*)^{-1} - (\Sigma_{\tilde{y}}^\theta)^{-1}\| + \|\Delta_{\tilde{z}\tilde{y}}^\theta ((\Sigma_{\tilde{y}}^\theta)^*)^{-1}\| \|\tilde{y}^\theta\| \\ &\leq \|\Sigma_{\tilde{z}\tilde{y}}^\theta\| \|((\Sigma_{\tilde{y}}^\theta)^*)^{-1} - (\Sigma_{\tilde{y}}^\theta)^{-1}\| \|\tilde{y}^\theta\| \\ &\quad + \|\Delta_{\tilde{z}\tilde{y}}^\theta\| \|((\Sigma_{\tilde{y}}^\theta)^*)^{-1}\| \|\tilde{y}^\theta\| \end{aligned} \quad (68)$$

where we define $\Delta_{\tilde{z}\tilde{y}}^\theta = (\Sigma_{\tilde{z}\tilde{y}}^\theta)^* - \Sigma_{\tilde{z}\tilde{y}}^\theta$ and $\Delta_{\tilde{y}}^\theta = (\Sigma_{\tilde{y}}^\theta)^* - \Sigma_{\tilde{y}}^\theta$. The notation $\|\cdot\|$ denotes the operator norm for matrices.

The rest of the proof is based on studying the rates of convergence of the terms obtained in (68). We recall from the proof of Theorem 1 that $C_{\zeta^0} = \|\Sigma_{\tilde{x}}\|_F^2 + \text{tr}(\Sigma_{\tilde{x}})^2 = O(N^2 T^2 d^4)$, which implies $\|\tilde{y}^\theta\| = O(\sqrt{NT} d^2)$. We observe that $\|\tilde{y}^\theta\|$ does not depend on the number of realizations L in (68). Meanwhile, although the norms $\|\Sigma_{\tilde{z}\tilde{y}}^\theta\|$ and $\|\Delta_{\tilde{z}\tilde{y}}^\theta\|$ of the covariance terms increase at rate $O(NT d^2)$ as the dimensions increase, this effect is typically expected to be neutralized by the inverse covariance terms in product with them in (68). Therefore, in the sequel, when analyzing the covariance terms in (68), we focus only on their dependence on the number of realizations L and do not consider their dependence on N , T and d .

Regarding their dependence on only L , the terms $\|\Sigma_{\tilde{z}\tilde{y}}^\theta\|$ and $\|((\Sigma_{\tilde{y}}^\theta)^*)^{-1}\|$ in (68) are of $O(1)$. Next, we have

$$\begin{aligned} \|\Delta_{\tilde{z}\tilde{y}}^\theta\| &\leq \|\Delta_{\tilde{z}\tilde{y}}^\theta\|_F = \|(\Sigma_{\tilde{z}\tilde{y}}^\theta)^* - \Sigma_{\tilde{z}\tilde{y}}^\theta\|_F \leq \|\Sigma_{\tilde{x}}^* - \Sigma_{\tilde{x}}\|_F \\ &= O\left(\frac{1}{\sqrt{L\delta}}\right) \end{aligned} \quad (69)$$

with probability at least $1 - \delta$ due to (67). Lastly, we study the term

$$\|((\Sigma_{\tilde{y}}^\theta)^*)^{-1} - (\Sigma_{\tilde{y}}^\theta)^{-1}\| = \|(\Sigma_{\tilde{y}}^\theta + \Delta_{\tilde{y}}^\theta)^{-1} - (\Sigma_{\tilde{y}}^\theta)^{-1}\|. \quad (70)$$

From Woodbury matrix identity, we have

$$(\Sigma_{\tilde{y}}^\theta + \Delta_{\tilde{y}}^\theta)^{-1} = (\Sigma_{\tilde{y}}^\theta)^{-1} - (\Sigma_{\tilde{y}}^\theta)^{-1} \left((\Delta_{\tilde{y}}^\theta)^{-1} + (\Sigma_{\tilde{y}}^\theta)^{-1} \right)^{-1} (\Sigma_{\tilde{y}}^\theta)^{-1}. \quad (71)$$

Using this in (70) we get

$$\begin{aligned} &\|((\Sigma_{\tilde{y}}^\theta)^*)^{-1} - (\Sigma_{\tilde{y}}^\theta)^{-1}\| \\ &= \|(\Sigma_{\tilde{y}}^\theta)^{-1} \left((\Delta_{\tilde{y}}^\theta)^{-1} + (\Sigma_{\tilde{y}}^\theta)^{-1} \right)^{-1} (\Sigma_{\tilde{y}}^\theta)^{-1}\| \\ &= \left\| (\Sigma_{\tilde{y}}^\theta)^{-1} \left(\Delta_{\tilde{y}}^\theta - \Delta_{\tilde{y}}^\theta ((\Sigma_{\tilde{y}}^\theta)^*)^{-1} \Delta_{\tilde{y}}^\theta \right) (\Sigma_{\tilde{y}}^\theta)^{-1} \right\| \\ &\leq \|(\Sigma_{\tilde{y}}^\theta)^{-1}\|^2 \|\Delta_{\tilde{y}}^\theta\| \|I - ((\Sigma_{\tilde{y}}^\theta)^*)^{-1} \Delta_{\tilde{y}}^\theta\| \end{aligned} \quad (72)$$

where the second equality is obtained by using the Woodbury matrix identity, this time for the matrices $(\Delta_{\tilde{y}}^\theta)^{-1}$ and $(\Sigma_{\tilde{y}}^\theta)^{-1}$. In (72), we observe that the terms $\|(\Sigma_{\tilde{y}}^\theta)^{-1}\|^2$ and $\|I - ((\Sigma_{\tilde{y}}^\theta)^*)^{-1} \Delta_{\tilde{y}}^\theta\|$ are of $O(1)$ as L increases. Meanwhile, similarly to (69), it can be shown that with probability at least $1 - \delta$,

$$\|\Delta_{\tilde{y}}^\theta\| = O\left(\frac{1}{\sqrt{L\delta}}\right) \quad (73)$$

which gives from (72)

$$\|((\Sigma_{\tilde{y}}^\theta)^*)^{-1} - (\Sigma_{\tilde{y}}^\theta)^{-1}\| = O\left(\frac{1}{\sqrt{L\delta}}\right). \quad (74)$$

Finally, combining the results (69) and (74) in (68) and recalling that $\|\tilde{y}^\theta\| = O(\sqrt{NT} d^2)$, we conclude that with probability at least $1 - \delta$,

$$\|(\tilde{z}^\theta)^* - (\tilde{z}^\theta)^0\| = O\left(\sqrt{\frac{NT d^2}{L\delta}}\right) \quad (75)$$

which finishes the proof. □

REFERENCES

- [1] B. Girault, P. Gonçalves, and E. Fleury, "Translation on graphs: An isometric shift operator," *IEEE Signal Processing Letters*, vol. 22, no. 12, pp. 2416–2420, Dec 2015.
- [2] N. Perraudin and P. Vandergheynst, "Stationary signal processing on graphs," *IEEE Transactions on Signal Processing*, vol. 65, no. 13, pp. 3462–3477, July 2017.
- [3] A. G. Marques, S. Segarra, G. Leus, and A. Ribeiro, "Stationary graph processes and spectral estimation," *IEEE Trans. Sig. Proc.*, vol. 65, no. 22, Nov 2017.
- [4] A. Loukas and N. Perraudin, "Stationary time-vertex signal processing," *EURASIP Journal on Advances in Signal Processing*, vol. 2019, no. 1, p. 36, 2019.
- [5] J. Mei and J. M. F. Moura, "Signal processing on graphs: Causal modeling of unstructured data," *IEEE Trans. Signal Process.*, vol. 65, no. 8, pp. 2077–2092, 2017.

- [6] E. Isufi, A. Loukas, N. Perraudin, and G. Leus, "Forecasting time series with VARMA recursions on graphs," *IEEE Trans. Signal Process.*, vol. 67, no. 18, pp. 4870–4885, 2019.
- [7] D. Zhou, O. Bousquet, T. N. Lal, J. Weston, and B. Schölkopf, "Learning with local and global consistency," in *Advances in Neural Inf. Proc. Sys.*, 2003, pp. 321–328.
- [8] A. Jung, A. O. Hero III, A. C. Mara, S. Jahromi, A. Heimowitz, and Y. C. Eldar, "Semi-supervised learning in network-structured data via total variation minimization," *IEEE Trans. Signal Process.*, vol. 67, no. 24, pp. 6256–6269, 2019.
- [9] P. Berger, G. Hannak, and G. Matz, "Graph signal recovery via primal-dual algorithms for total variation minimization," *IEEE J. Sel. Top. Signal Process.*, vol. 11, no. 6, pp. 842–855, 2017.
- [10] J. H. Giraldo, A. Mahmood, B. García-García, D. Thanou, and T. Bouwmans, "Reconstruction of time-varying graph signals via sobolev smoothness," *IEEE Trans. Signal Inf. Process. over Networks*, vol. 8, pp. 201–214, 2022.
- [11] J. Jiang, D. Tay, Q. Sun, and S. Ouyang, "Recovery of time-varying graph signals via distributed algorithms on regularized problems," *IEEE Trans. Signal Inf. Process. over Networks*, vol. 6, pp. 540–555, 2020.
- [12] K. Qiu, X. Mao, X. Shen, X. Wang, T. Li, and Y. Gu, "Time-varying graph signal reconstruction," *IEEE J. Sel. Top. Signal Process.*, vol. 11, no. 6, pp. 870–883, 2017.
- [13] P. Di Lorenzo, S. Barbarossa, P. Banelli, and S. Sardellitti, "Adaptive least mean squares estimation of graph signals," *IEEE Trans. Signal Inf. Process. over Networks*, vol. 2, no. 4, pp. 555–568, 2016.
- [14] P. Di Lorenzo, P. Banelli, E. Isufi, S. Barbarossa, and G. Leus, "Adaptive graph signal processing: Algorithms and optimal sampling strategies," *IEEE Trans. Signal Process.*, vol. 66, no. 13, pp. 3584–3598, 2018.
- [15] G. Yang, L. Yang, Z. Yang, and C. Huang, "Efficient node selection strategy for sampling bandlimited signals on graphs," *IEEE Trans. Signal Process.*, vol. 69, pp. 5815–5829, 2021.
- [16] L. F. O. Chamon and A. Ribeiro, "Greedy sampling of graph signals," *IEEE Trans. Signal Process.*, vol. 66, no. 1, pp. 34–47, 2018.
- [17] E. Isufi, P. Banelli, P. Di Lorenzo, and G. Leus, "Observing and tracking bandlimited graph processes from sampled measurements," *Signal Process.*, vol. 177, p. 107749, 2020.
- [18] B. Girault, "Stationary graph signals using an isometric graph translation," in *2015 23rd European Signal Processing Conference (EUSIPCO)*, Aug 2015, pp. 1516–1520.
- [19] H. Lütkepohl, *New introduction to multiple time series analysis*. Springer, 2005.
- [20] A. Jung, "Learning the conditional independence structure of stationary time series: A multitask learning approach," *IEEE Trans. Signal Process.*, vol. 63, no. 21, pp. 5677–5690, 2015.
- [21] N. Perraudin, A. Loukas, F. Grassi, and P. Vandergheynst, "Towards stationary time-vertex signal processing," in *Proc. IEEE ICASSP*, 2017, pp. 3914–3918.
- [22] F. Grassi, A. Loukas, N. Perraudin, and B. Ricaud, "A time-vertex signal processing framework: Scalable processing and meaningful representations for time-series on graphs," *IEEE Transactions on Signal Processing*, vol. 66, no. 3, pp. 817–829, Feb 2018.
- [23] E. Isufi, A. Loukas, A. Simonetto, and G. Leus, "Separable autoregressive moving average graph-temporal filters," in *Proc. 24th EUSIPCO*, 2016, pp. 200–204.
- [24] M. Hayes, *Statistical Digital Signal Processing and Modeling*. Wiley, 1996.
- [25] E. T. Güneyi, A. Canbolat, and E. Vural, "Learning parametric time-vertex graph processes from incomplete realizations," in *IEEE Int. Workshop Machine Learning for Signal Processing*, 2021.
- [26] D. I. Shuman, S. K. Narang, P. Frossard, A. Ortega, and P. Vandergheynst, "The emerging field of signal processing on graphs: Extending high-dimensional data analysis to networks and other irregular domains," *IEEE Signal Processing Magazine*, vol. 30, no. 3, pp. 83–98, May 2013.
- [27] M. Grant and S. Boyd, "CVX: Matlab software for disciplined convex programming, version 2.1," Mar. 2014.
- [28] —, "Graph implementations for nonsmooth convex programs," in *Recent Advances in Learning and Control*. Springer-Verlag Limited, 2008, pp. 95–110.
- [29] R. H. Tütüncü, K. C. Toh, and M. J. Todd, "SDPT3 — a MATLAB software package for semidefinite programming, version 1.3," vol. 11:1–4, pp. 545–581, 1999.
- [30] —, "Solving semidefinite-quadratic-linear programs using SDPT3," vol. 95:2, pp. 189–217, 2003.
- [31] A. Arguez et al., "NOAA's 1981-2020 U.S. climate normals: An overview," in *Proc. Bull. Amer. Meteorol. Soc.*, 2012, pp. 1687–1697.
- [32] "COVID-19 coronavirus pandemic data." [Online]. Available: <https://www.worldometers.info/coronavirus/>
- [33] "Eurostat: An official website of the European Union." [Online]. Available: <https://ec.europa.eu/eurostat>